Optical Engineering

OpticalEngineering.SPIEDigitalLibrary.org

Aperture averaging in multiple-input single-output free-space optical systems

Muhsin C. Gökçe
Yahya Baykal
Canan Kamacıoğlu
Murat Uysal

SPIE.

Aperture averaging in multiple-input single-output free-space optical systems

Muhsin C. Gökçe,[a] Yahya Baykal,[b,*] Canan Kamacıoğlu,[a] and Murat Uysal[c]
[a]Çankaya University, Department of Electronic and Communication Engineering, Yukarıyurtçu Mahallesi Mimar Sinan Caddesi Etimesgut, Ankara 06790, Turkey
[b]Çankaya University, Department of Electrical-Electronics Engineering, Yukarıyurtçu Mahallesi Mimar Sinan Caddesi. Etimesgut, Ankara 06790, Turkey
[c]Özyeğin University, Department of Electrical and Electronics Engineering, Nişantepe Mevki Orman Sokak No:13 Alemdağ/Çekmeköy, İstanbul 34794, Turkey

Abstract. Multiple-input single-output systems are employed in free-space optical links to mitigate the degrading effects of atmospheric turbulence. We formulate the power scintillation as a function of transmitter and receiver coordinates in the presence of weak atmospheric turbulence by using the extended Huygens–Fresnel principle. Then the effect of the receiver–aperture averaging is quantified. To get consistent results, parameters are chosen within the range of validity of the wave structure functions. Radial array beams and a Gaussian weighting aperture function are used at the transmitter and the receiver, respectively. It is observed that the power scintillation decreases when the source size, the ring radius, the receiver–aperture radius, and the number of array beamlet increase. However, increasing the number of array beamlets to more than three seems to have negligible effect on the power scintillation. It is further observed that the aperture averaging effect is stronger when radial array beams are employed instead of a single Gaussian beam. [DOI: 10.1117/1.OE.54.6.066103]

Keywords: Multiple-input single-output systems; free-space optical communication; optical wave propagation; power scintillation; aperture averaging.

Paper 150247P received Feb. 26, 2015; accepted for publication May 27, 2015; published online Jun. 25, 2015.

1 Introduction

Atmospheric turbulence is one of the major performance limiting factors in free-space optical (FSO) communication links. Receiver–aperture averaging is commonly used to reduce the turbulence-induced scintillation effect. The performance improvement of aperture averaging is typically quantified by the "aperture averaging factor" which is defined as the ratio of scintillation index of a finite-sized aperture to a point aperture. The aperture averaging factor for the plane wave intensity fluctuations is derived by Tatarskii.[1] A similar performance study for a beam wave is also reported.[2] A flattened Gaussian beam with a misaligned circular transmitter aperture in the turbulent atmosphere has been further examined.[3,4] The aperture averaging factor for Gaussian beams has been analyzed in weak and moderate turbulence conditions by using the statistics of the exponentiated Weibull distribution family.[5] The scintillation index of a flat-topped beam in weak turbulence is formulated and the aperture averaging effect is quantified under a flat-topped incidence.[6] For an annular beam incidence, the scintillation index in a weakly turbulent atmosphere is derived at the receiver with a Gaussian aperture and the aperture averaging factor is evaluated.[7]

The employment of multiple transmitter and receiver apertures for spatial diversity in FSO systems provides additional advantages over their single-input single-output (SISO) counterparts and there has been growing literature on spatial diversity,[8–18] which is elaborated below. One special case of these systems is known as the multiple-input single-output (MISO) system, where the use of multiple transmit apertures can help the system to overcome the limitations on the transmit optical power.[8,9] The ergodic channel capacity of an MISO FSO link is investigated[10] and it is demonstrated that the capacity improves with the increasing number of transmit apertures. The outage probability of MISO FSO links is derived under the assumption of direct detection receivers and binary pulse position modulation.[8,11] The diversity gain order of FSO communication systems operating in log–normal turbulence-fading channels is quantified.[12] The bit error rate performance of MISO FSO systems with and without channel state information in both spatially correlated and uncorrelated channels is investigated.[13]

The existing works summarized above for the spatial diversity systems have mainly assumed a plane wave, which is a theoretical assumption of the wave propagation that remains unrealistic for practical implementation. For this reason, there is a considerable interest in using realistic beamshapes.[14–18] For example, using a Gaussian beams array, i.e., a number of Gaussian beams which come together with a specific distance at the transmitter and a point detector at the receiver, on-axis scintillation of MISO systems has been examined by using the extended Huygens–Fresnel principle.[14] A similar study has been reported by using the Rytov method.[15] Furthermore, the propagation factor, which is a common measure of the beam quality of a Gaussian beams array, is investigated for MISO systems.[16] Field correlation analysis of MISO system with a Gaussian beams array is also evaluated for heterodyne detection.[17] Finally, the on-axis

*Address all correspondence to: Yahya Baykal, E-mail: y.baykal@cankaya.edu.tr

0091-3286 /2015/$25.00

scintillation index is formulated for MISO FSO systems with overlapping Gaussian beams and a point detector.[18] In this paper, we consider an MISO FSO system consisting of a radial transmit array with Gaussian sources and a finite-sized detector. We derive the average received intensity as a function of the receiver coordinates in the presence of weak atmospheric turbulence by using the extended Huygens–Fresnel principle. This allows us to calculate the power scintillation index and the receiver–aperture averaging factor. Based on these performance metrics, we examine the effect of several parameters such as the receiver–aperture radius, ring radius, number of beamlets, and the source size on the scintillations and thus the receiver–aperture averaging factor.

2 System Model and Performance Analysis

2.1 *System Model*

We consider an MISO FSO system as illustrated in Fig. 1. We assume a radial laser transmit array consisting of N Gaussian beamlets, with α_s being the source size of the Gaussian beamlets, i.e., the beam-waist radius of each beamlet. Since the Gaussian beamlets are taken to be collimated, the beam-waist radius and the Gaussian source size are equal to each other at the transmitter plane. Beamlets are located equi-distant from each other on a ring with radius r_0. At the receiver side, there is a finite aperture receiver with radius R_r that has a Gaussian aperture function.

2.2 *Calculation of the Average Power*

We first calculate the average intensity at the receiver plane, which is then used to calculate the average power $\langle P\rangle$ and the average of the square of the power $\langle P^2\rangle$. This enables us to calculate the power scintillation index and the receiver–aperture averaging factor.

The source field expression for a laser array with Gaussian sources can be expressed as[14]

$$u(s_x,s_y)=\sum_{n=1}^{N}\exp\{-k\alpha_n[s_x^2+s_y^2 - 2r_0(s_x\cos\varphi_n+s_y\sin\varphi_n-0.5r_0)]\}, \quad (1)$$

where $\alpha_n=1/(2k\alpha_s^2)$, $\varphi_n=2\pi(n-1)/N$, $\mathbf{s}=(s_x,s_y)$ is the source transverse coordinate, $k=2\pi/\lambda$ is the wave number, and λ is the wavelength. From the extended Huygens–Fresnel integral, the average intensity at the receiver plane is found to be[1]

$$\langle I(\mathbf{p})\rangle=\frac{1}{(\lambda L)^2}\int_{-\infty}^{\infty}\int_{-\infty}^{\infty}\int_{-\infty}^{\infty}\int_{-\infty}^{\infty}\mathrm{d}\mathbf{s}_1^2\mathrm{d}\mathbf{s}_2^2u(\mathbf{s}_1)u^*(\mathbf{s}_2) \times\exp\left\{\frac{jk}{2L}[(\mathbf{p}-\mathbf{s}_1)^2-(\mathbf{p}-\mathbf{s}_2)^2]-\rho_0^{-2}(\mathbf{s}_1-\mathbf{s}_2)^2\right\}, \quad (2)$$

where $j=\sqrt{-1}$, $*$ is the complex conjugate, $\mathbf{p}=(p_x,p_y)$ is the receiver transverse coordinate, $\rho_0=(0.546C_n^2k^2L)^{-3/5}$ is the coherence length of a spherical wave propagating in the turbulent medium, and C_n^2 is the index-of-refraction structure constant. In the extended Huygens–Fresnel principle, the field at the receiver is obtained by the convolution of the spherical wave response of the turbulent medium and the source field. Equation (2) is found by employing the extended Huygens–Fresnel principle. This is the reason why in Eq. (2), the spatial coherence length ρ_0 is taken for the spherical wave. Solving Eq. (2) by the repeated use of Eq. 3.323.2,[19] we obtain

$$\langle I(\mathbf{p},L)\rangle=\frac{\pi^2}{(\lambda L)^2}\sum_{n=1}^{N}\sum_{m=1}^{M}\frac{1}{t_1^2t_2^2}\exp(-r_0^2\alpha_{sn}^{-2}) \times\exp\left(-\frac{k^2}{4t_1^2L^2}p_x^2+\frac{r_0^2\cos^2\varphi_n}{4t_1^2\alpha_s^4}-\frac{r_0\cos\varphi_n}{2t_1^2\alpha_s^2}\frac{jk}{L}p_x\right) \times\exp\left(\frac{w_{2x}^2}{4t_2^2}\right)\exp\left(\frac{w_{2y}^2}{4t_2^2}\right) \times\exp\left(-\frac{k^2}{4t_1^2L^2}p_y^2+\frac{r_0^2\sin^2\varphi_n}{4t_1^2\alpha_s^4}-\frac{r_0\sin\varphi_n}{2t_1^2\alpha_s^2}\frac{jk}{L}p_y\right), \quad (3)$$

where

$$t_1=(0.5\alpha_s^{-2}-0.5jkL^{-1}+\rho_0^{-2})^{0.5},$$
$$t_2=(0.5\alpha_s^{-2}+0.5jkL^{-1}+\rho_0^{-2}-t_1^{-2}\rho_0^{-4})^{1/2},$$
$$w_{2x}=r_0\left(\cos\varphi_m\frac{1}{\alpha_s^2}+\cos\varphi_n\frac{1}{t_1^2\alpha_s^2\rho_0^2}\right)+\frac{jkp_x}{L}\left(1-\frac{1}{t_1^2\rho_0^2}\right),$$
$$w_{2y}=r_0\left(\sin\varphi_m\frac{1}{\alpha_s^2}+\sin\varphi_n\frac{1}{t_1^2\alpha_s^2\rho_0^2}\right)+\frac{jkp_y}{L}\left(1-\frac{1}{t_1^2\rho_0^2}\right).$$

The average power detected by a finite-sized receiver having a Gaussian aperture function is calculated as

$$\langle P\rangle=\int_{-\infty}^{\infty}\int_{-\infty}^{\infty}\langle I(\mathbf{p})\rangle\exp\left(-\frac{|\mathbf{p}|^2}{R_r^2}\right)\mathrm{d}^2\mathbf{p}, \quad (4)$$

where R_r is the radius of the receiver aperture. Substituting Eq. (3) into Eq. (4) and performing the integrations, we obtain

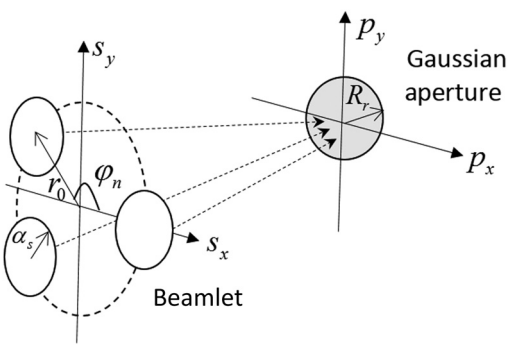

Fig. 1 Schematic illustration of multiple-input single-output (MISO) free-space optical (FSO) system for $N=3$ radially located sources at the transmitter and an aperture with radius R_r at the receiver.

$$\langle P\rangle = \frac{\pi^3}{(\lambda L)^2}\sum_{n=1}^{N}\sum_{m=1}^{M}\exp(-r_0^2\alpha_s^{-2})\frac{1}{t_1^2t_2^2t_p^2}$$
$$\times\exp\left[\frac{r_0^2\cos^2\varphi_n}{4t_1^2\alpha_s^4}+\frac{r_0^2}{4t_2^2}\left(\cos\varphi_m\frac{1}{\alpha_s^2}+\cos\varphi_n\frac{1}{t_1^2\alpha_s^2\rho_0^2}\right)^2\right]$$
$$\times\exp\left(\frac{w_{px}^2+w_{py}^2}{4t_p^2}\right)$$
$$\times\exp\left[\frac{r_0^2\sin^2\varphi_n}{4t_1^2\alpha_s^4}+\frac{r_0^2}{4t_2^2}\left(\sin\varphi_m\frac{1}{\alpha_s^2}+\sin\varphi_n\frac{1}{t_1^2\alpha_s^2\rho_0^2}\right)^2\right], \tag{5}$$

where

$$t_p^2 = R_r^{-2}+\frac{k^2}{4t_1^2L^2}+\frac{k^2(1-t_1^{-2}\rho_0^{-2})^2}{4t_2^2L^2},$$
$$w_{px} = \frac{jk}{L}\left[-\frac{r_0\cos\varphi_n}{2t_1^2\alpha_s^2}+\frac{r_0}{2t_2^2}\left(\frac{\cos\varphi_m}{\alpha_s^2}+\frac{\cos\varphi_n}{t_1^2\alpha_s^2\rho_0^2}\right)\left(1-\frac{1}{t_1^2\rho_0^2}\right)\right],$$
$$w_{py} = \frac{jk}{L}\left[-\frac{r_0\sin\varphi_n}{2t_1^2\alpha_s^2}+\frac{r_0}{2t_2^2}\left(\frac{\sin\varphi_m}{\alpha_s^2}+\frac{\sin\varphi_n}{t_1^2\alpha_s^2\rho_0^2}\right)\left(1-\frac{1}{t_1^2\rho_0^2}\right)\right].$$

The average of the square of the power as detected by a finite-sized receiver having a Gaussian aperture function is found as

$$\langle P^2\rangle = \int_{-\infty}^{\infty}\int_{-\infty}^{\infty}\int_{-\infty}^{\infty}\int_{-\infty}^{\infty}\langle I(\mathbf{p_1})I(\mathbf{p_2})\rangle$$
$$\times\exp\left(-\frac{|\mathbf{p_1}|^2+|\mathbf{p_2}|^2}{R_r^2}\right)\mathrm{d}^2\mathbf{p_1}\mathrm{d}^2\mathbf{p_2}. \tag{6}$$

The derivation and the resulting expression for $\langle P^2\rangle$ are provided in the Appendix.

2.3 *Performance Metrics*

In this paper, we adopt two performance metrics, namely, power scintillation and the aperture averaging factor. The power scintillation quantifies fluctuations in the received irradiance and is defined as[20]

$$m_p^2 = \frac{\langle(P-\langle P\rangle)^2\rangle}{\langle P\rangle^2} = \frac{\langle P^2\rangle}{\langle P\rangle^2}-1. \tag{7}$$

In the region of weak fluctuations, m_p^2 takes typical values that are much less than unity. On the other hand, the receiver–aperture averaging factor quantifies the relative gain in power scintillation with respect to a point receiver. It is defined as

$$G_R = \frac{m_p^2}{m_p^2\big|_{R_r=0}}, \tag{8}$$

where $m_p^2|_{R_r=0}$ is the power scintillation index for a point aperture, i.e., the intensity scintillation index. For an effective aperture averaging, the power scintillation detected by a finite-sized aperture must be lower than the scintillation detected by a point aperture.

3 Numerical Results

In this section, we present numerical results for power scintillation and the aperture averaging factor derived in the previous section based on Eqs. (7) and (8). We are particularly interested in quantifying the effect of the receiver–aperture radius, the ring radius, the number of beamlets, and the source size on these performance metrics. We note that the parameters are chosen within the validity range of the wave structure function which depends on $(\lambda L)^{1/2} \gg |\mathbf{s_d}| \gg l_0$ for the case of $C_n^2 =$ constant, with l_0 being the inner scale of turbulence. Thus, system parameters of the MISO system are chosen within the range of validity of the wave structure functions that limit the employed ring diameters and the beam diameters to physically small dimensions. We assume that the wavelength is chosen as $\lambda = 1.55$ μm. In our evaluations, the beamlets forming the source array are taken to be collimated so that they are co-aligned in the transmit plane with the divergence covering the Gaussian aperture in the receiver plane.

In Fig. 2, we illustrate the variation of the power scintillation against the ring radius for different numbers of beamlets. Specifically, we assume $N = 1, 2, 3$, a receiver aperture

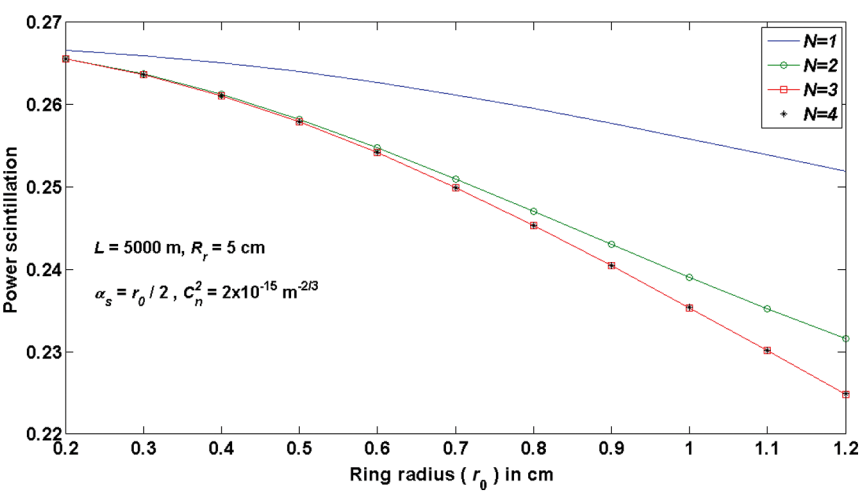

Fig. 2 The power scintillation versus the ring radius r_0 assuming $L = 5000$ m, $R_r = 5$ cm, $C_n^2 = 2\times10^{-15}$ m$^{-2/3}$ for different number of beamlets N and the source size α_s values.

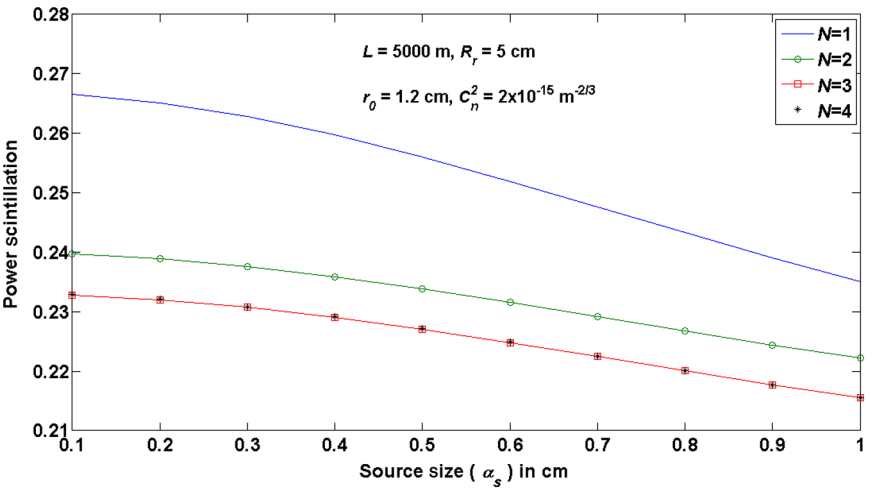

Fig. 3 The power scintillation versus the source size α_s at $L = 5000$ m, $R_r = 5$ cm, $r_0 = 1.2$ cm, $C_n^2 = 2 \times 10^{-15}$ m$^{-2/3}$ for different N values.

radius of $R_r = 5$ cm, a link distance $L = 5000$ m, and a structure constant of the atmosphere $C_n^2 = 2 \times 10^{-15}$ m$^{-2/3}$. The transmit aperture radius is assumed to linearly change with the ring radius $\alpha_s = r_0/2$ cm to prevent overlapping. It is observed that the power scintillation decreases as the ring radius and number of beamlets increase.

In Fig. 3, we keep a transmitter ring radius of $r_0 = 1.2$ cm constant and illustrate the variation of power scintillation with respect to source size α_s assuming beamlet numbers of $N = 1, 2, 3$. We consider a system with a link distance $L = 5000$ m, receiver–aperture radius of $R_r = 5$ cm and structure constant $C_n^2 = 2 \times 10^{-15}$ m$^{-2/3}$. It is observed that as the source size increases, the scintillation decreases. Similar results are also pointed out in our earlier work,[21] which emphasize that significant scintillation reduction can be obtained through proper parameter choices. The change in the source size, i.e., the beam-waist, also causes a change in the beam divergence which will result in large or small beam-steering effects originating from atmospheric turbulence. Since in our formulation the second-order effects are also involved through the average power, our presented model accounts for the beam-steering as well.

In Figs. 4 and 5, we plot the variation of the power scintillation with respect to the number of beamlets in an MISO FSO system and investigate the effects of various system parameters on the performance. In Fig. 4, we assume a link distance of $L = 5000$ m, transmitter ring radius of $r_0 = 1$ cm, receiver–aperture radius of $R_r = 5$ cm, structure constant $C_n^2 = 2 \times 10^{-15}$ m$^{-2/3}$, and α_s takes values between 0.5 and 0.8 cm. It is observed that the power scintillation decreases when the number of beamlets increases. Furthermore, scintillation reduction is obtained as the source size increases. It is also observed that the power scintillation starts to attain the same values when $N > 3$. In Fig. 5, we assume a link distance of $L = 5000$ m, $\alpha_s = 0.5$ cm, structure constant $C_n^2 = 2 \times 10^{-15}$ m$^{-2/3}$, receiver–aperture radius R_r takes values of 5 and 6 cm, while the transmitter ring radius r_0 is set as 0.75, 1, 1.25, and 1.5 cm. It is observed that as the transmitter ring radius increases, the power scintillation index decreases. Also, an increase in α_s results in a reduction in the scintillations.

In Fig. 6, we illustrate the averaging factor using Eq. (8) and demonstrate its change with respect to the receiver–aperture radius R_r. We assume a link distance of $L = 5000$ m,

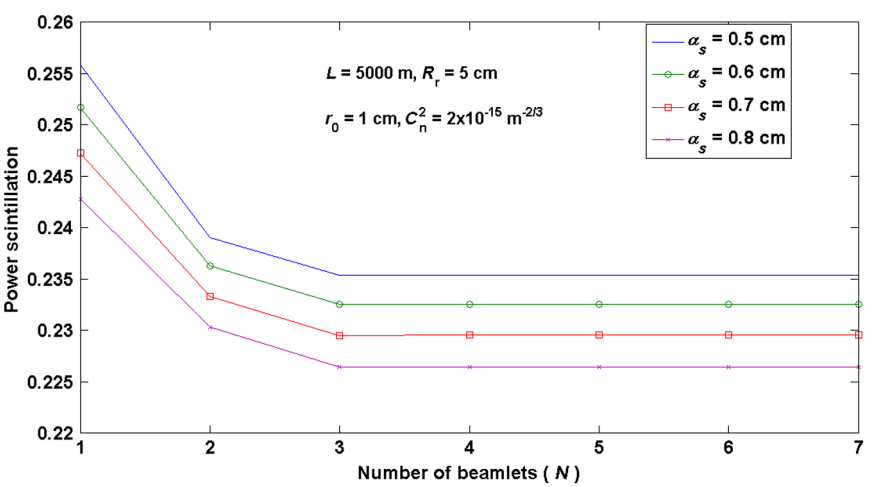

Fig. 4 The power scintillation versus the number of beamlets N at $L = 5000$ m, $R_r = 5$ cm, $r_0 = 1$ cm, $C_n^2 = 2 \times 10^{-15}$ m$^{-2/3}$ for different α_s values.

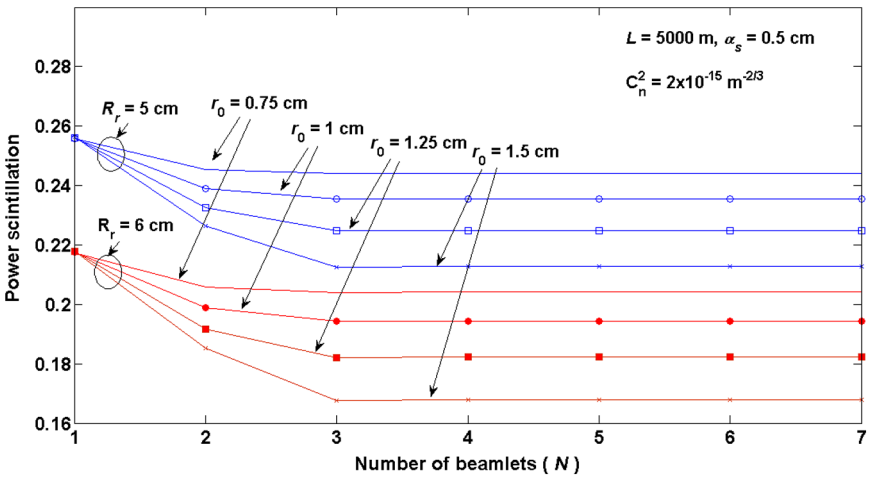

Fig. 5 The power scintillation versus the number of beamlets N at $L = 5000$ m, $\alpha_s = 05$ cm, $C_n^2 = 2 \times 10^{-15}$ m$^{-2/3}$ for different r_0 and R_r values.

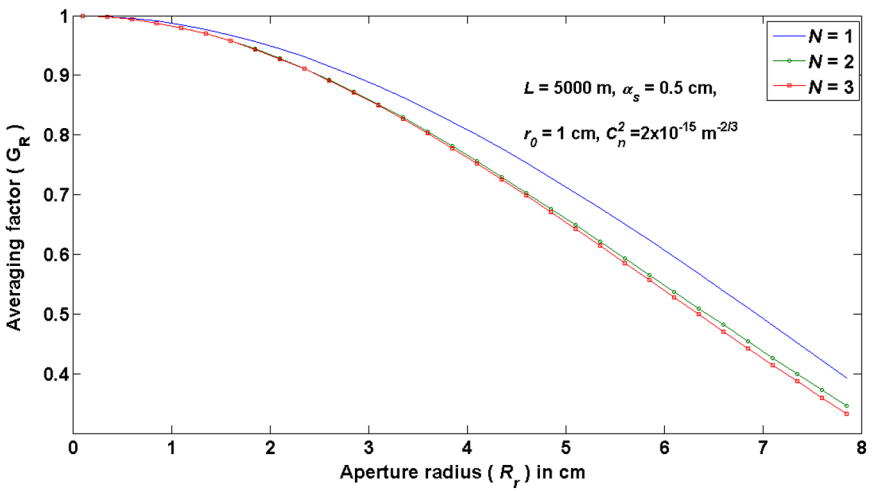

Fig. 6 The receiver–aperture averaging factor G_R versus the radius of the receiver aperture radius R_r at $L = 5000$ m, $\alpha_s = 0.5$ cm, $r_0 = 1$ cm, $C_n^2 = 2 \times 10^{-15}$ m$^{-2/3}$ for different N values.

transmitter ring radius of $r_0 = 1$ cm, $\alpha_s = 0.5$ cm, and structure constant $C_n^2 = 2 \times 10^{-15}$ m$^{-2/3}$. It is observed from Fig. 6 that the aperture averaging factor decreases with an increase in the receiver–aperture radius. Furthermore, when the number of transmitter beamlets is increased, the scintillation index is decreased which, in turn, causes the aperture averaging factor to decrease. From the figures in this section, it is seen that no additional power scintillation index benefit is gained when more than three beamlets are used. For example, in Figs. 4 and 5, the power scintillation index fairly abruptly becomes a very flat line. This is attributed to the situation where, as the number of beamlets reaches a certain value, the footprint of the received optical beam that falls within the receiver aperture does not show much variation, thus an additional beamlet in the array does not cause further change in the scintillations.

Our results indicate that the overall aperture averaging effect is a combination of the reduction in the scintillations due to multibeaming and due to the finite receiver aperture. In the absence of turbulence, our equations yield zero scintillations, thus aperture averaging is of no concern when there is no turbulence.

4 Conclusion

In this paper, we examined the effects of aperture averaging in an MISO FSO system. It is found that the power scintillation decreases as the ring radius and the number of beamlets increase. The effect of the ring radius to reduce the power scintillation is more pronounced for a larger number of beamlets. It is also observed that the power scintillation changes negligibly when N becomes larger than 3. This is thought to originate due to the situation where, at a sufficiently large number of beamlets, the received optical beam within the receiver–aperture area does not show much variation with the addition of another beamlet. It is also found that the increase in the source sizes decreases the power scintillation. The power scintillation decreases as the receiver–aperture radius increases. An increase in the transmitter ring radius also causes a decrease in the scintillation index. The aperture averaging factor decreases with an increase in the receiver–aperture radius. The effect is stronger as the number of beamlets increases.

Appendix

This appendix shows the calculation of $\langle P^2\rangle$. First, we need to calculate $\langle I(\mathbf{p_1})I(\mathbf{p_2})\rangle$ given by

$$\langle I(\mathbf{p_1})I(\mathbf{p_2})\rangle = \frac{1}{(\lambda L)^4}\int_{-\infty}^{\infty}\int_{-\infty}^{\infty}\mathrm{d}^2\mathbf{s}_1\int_{-\infty}^{\infty}\int_{-\infty}^{\infty}\mathrm{d}^2\mathbf{s}_2\int_{-\infty}^{\infty}\int_{-\infty}^{\infty}\mathrm{d}^2\mathbf{s}_3\int_{-\infty}^{\infty}\int_{-\infty}^{\infty}\mathrm{d}^2\mathbf{s}_4 u(\mathbf{s}_1)u^*(\mathbf{s}_2)u(\mathbf{s}_3)u^*(\mathbf{s}_4)$$
$$\times\exp\left[\frac{jk}{2L}(|\mathbf{p_1}-\mathbf{s_1}|^2-|\mathbf{p_1}-\mathbf{s_2}|^2+|\mathbf{p_2}-\mathbf{s_3}|^2-|\mathbf{p_2}-\mathbf{s_4}|^2)\right]$$
$$\times\langle\exp[\psi(\mathbf{s}_1,\mathbf{p_1})+\psi^*(\mathbf{s}_2,\mathbf{p_1})+\psi(\mathbf{s}_3,\mathbf{p_2})+\psi^*(\mathbf{s}_4,\mathbf{p_2})]\rangle, \tag{9}$$

where $\psi(\mathbf{s},\mathbf{p})$ is the Rytov solution of the random part of the complex phase of a spherical wave propagating from the source point $(\mathbf{s}, z=0)$ to the receiver point $(\mathbf{p}, z=L)$ with z being the propagation axis. The fourth-order medium coherence function given in the last line of Eq. (9) is used as the given in Ref. 2. Employing Eq. (1) and the related equations of Ref. 2 in Eq. (9) and using the resulting Eq. (9) in Eq. (6), the equation for $\langle P^2\rangle$ is obtained. Applying Eq. 3.323.2 of Ref. 19 which is $\int_{-\infty}^{\infty}\mathrm{d}x\,\exp(-t^2x^2\pm qx) = (\pi^{0.5}/t)\exp[q^2/(4\,t^2)]$, $[\mathrm{Re}(t^2)>0]$ and performing the 8-fold integration over the source transverse coordinates and the 4-fold integration over the transverse receiver coordinates, we find

$$\langle P^2\rangle = \frac{\exp(4\sigma_{\chi_s}^2)}{(\lambda L)^4}\sum_{n=1}^{N}\sum_{m=1}^{N}\sum_{l=1}^{N}\sum_{o=1}^{N}\exp[-r_0^2k(\alpha_n+\alpha_m+\alpha_l+\alpha_o)]\frac{\pi^6}{\beta_1^2\beta_2^2\beta_3^2\beta_4^2\beta_{1p}^2\beta_{2p}^2}\exp\left(\frac{JJ_x^2}{4\beta_{1p}^2}\right)$$
$$\times\exp\left(\frac{JJ_y^2}{4\beta_{1p}^2}\right)\exp\left(\frac{q_{2px}^2}{4\beta_{2p}^2}\right)\exp\left(\frac{q_{2py}^2}{4\beta_{2p}^2}\right)\exp\left(\frac{\mathrm{AA}_x^2}{4\beta_3^2}\right)\exp\left(\frac{\mathrm{AA}_y^2}{4\beta_3^2}\right)\exp\left(\frac{CC_x^2}{4\beta_4^2}\right)\exp\left(\frac{CC_y^2}{4\beta_4^2}\right)$$
$$\times\exp\left(\frac{\cos^2\varphi_n k^2\alpha_n^2r_0^2}{\beta_1^2}+\cos^2\varphi_n k^2\alpha_n^2r_0^2\frac{1}{\beta_2^2\beta_1^4\rho_0^4}\right)\exp\left(\frac{k^2\alpha_m^2r_0^2\cos^2\varphi_m}{\beta_2^2}+\cos\varphi_n k\alpha_n r_0\frac{2}{\beta_2^2\beta_1^2\rho_0^2}k\alpha_m r_0\cos\varphi_m\right)$$
$$\times\exp\left(\frac{\sin^2\varphi_n k^2\alpha_n^2r_0^2}{\beta_1^2}+\sin^2\varphi_n k^2\alpha_n^2r_0^2\frac{1}{\beta_2^2\beta_1^4\rho_0^4}\right)\exp\left(\frac{k^2\alpha_m^2r_0^2\sin^2\varphi_m}{\beta_2^2}+\sin\varphi_n k\alpha_n r_0\frac{2}{\beta_2^2\beta_1^2\rho_0^2}k\alpha_m r_0\sin\varphi_m\right), \tag{10}$$

where

$$\beta_1^2 = k\alpha_n-\frac{jk}{2L}+\frac{2}{\rho_0^2}-T,\qquad \beta_2^2 = -\frac{1}{\beta_1^2\rho_0^4}+\theta_1^2,\qquad \beta_3^2 = -\frac{1}{\beta_2^2}\left(\frac{1}{\rho_0^2}-\frac{T}{\beta_1^2\rho_0^2}\right)^2-\frac{T^2}{\beta_1^2}+\varsigma_1^2,$$
$$\beta_4^2 = -\frac{1}{\beta_3^2}\left[\frac{1}{\beta_2^2}\left(\frac{1}{\rho_0^2}-\frac{T}{\beta_1^2\rho_0^2}\right)\left(\frac{1}{\beta_1^2\rho_0^4}-R\right)-\frac{T}{\beta_1^2\rho_0^2}+\frac{1}{\rho_0^2}\right]^2-\frac{1}{\beta_2^2}\left(\frac{1}{\beta_1^2\rho_0^4}-R\right)^2-\frac{1}{\beta_1^2\rho_0^4}+\xi_1^2,$$

$$R=\frac{j}{\rho_{\chi S}^2}+\frac{1}{\rho_x^2},\quad T=-\frac{j}{\rho_{\chi S}^2}+\frac{1}{\rho_x^2},$$
$$\theta_1^2=k\alpha_m+\frac{jk}{2L}+\frac{2}{\rho_0^2}-R,\ \varsigma_1^2=k\alpha_l-\frac{jk}{2L}+\frac{2}{\rho_0^2}-T,\ \ \xi_1^2=k\alpha_o+\frac{jk}{2L}+\frac{2}{\rho_0^2}-R,$$
$$\beta_{1p}^2=\frac{1}{R_r^2}-\frac{1}{4\beta_1^2}\left(-\frac{jk}{L}-\frac{1}{\rho_0^2}+T\right)^2-\frac{1}{4\beta_2^2}\left[\left(-\frac{jk}{L}-\frac{1}{\rho_0^2}+T\right)\frac{1}{\beta_1^2\rho_0^2}+\frac{jk}{L}-\frac{1}{\rho_0^2}+R\right]^2$$
$$-\frac{1}{4\beta_3^2}\left\{\frac{1}{\beta_2^2}\left[\left(-\frac{jk}{L}-\frac{1}{\rho_0^2}+T\right)\frac{1}{\beta_1^2\rho_0^2}+\frac{jk}{L}-\frac{1}{\rho_0^2}+R\right]\left(\frac{1}{\rho_0^2}-\frac{T}{\beta_1^2\rho_0^2}\right)-\frac{1}{\beta_1^2}\left(-\frac{jk}{L}-\frac{1}{\rho_0^2}+T\left(\frac{1}{\rho_0^2}-\frac{T}{\beta_1^2\rho_0^2}\right)T+\frac{1}{\rho_0^2}-T\right\}^2-\frac{B^2}{4\beta_4^2}+\frac{2}{\rho_0^2}-(T+R),$$

$$\beta_{2p}^2 = \frac{1}{R_r^2}-\frac{1}{4\beta_1^2}\left(\frac{1}{\rho_0^2}-T\right)^2-\frac{1}{4\beta_2^2}\left[\frac{1}{\beta_1^2\rho_0^2}\left(\frac{1}{\rho_0^2}-T\right)+\frac{1}{\rho_0^2}-R\right]^2$$
$$-\frac{1}{4\beta_3^2}\left\{\frac{1}{\beta_2^2}\left[\frac{1}{\beta_1^2\rho_0^2}\left(\frac{1}{\rho_0^2}-T\right)+\frac{1}{\rho_0^2}-R\right]\left(\frac{1}{\rho_0^2}-\frac{T}{\beta_1^2\rho_0^2}\right)-\frac{jk}{L}-\frac{1}{\rho_0^2}+T-\frac{T}{\beta_1^2}\left(\frac{1}{\rho_0^2}-T\right)\right\}^2-\frac{D^2}{4\beta_4^2}+\frac{2}{\rho_0^2}-(T+R)-\frac{KK^2}{4\beta_{1p}^2},$$

$$B = \frac{1}{\beta_3^2}\left\{\frac{1}{\beta_2^2}\left[\left(-\frac{jk}{L}-\frac{1}{\rho_0^2}+T\right)\frac{1}{\beta_1^2\rho_0^2}+\frac{jk}{L}-\frac{1}{\rho_0^2}+R\right]\left(\frac{1}{\rho_0^2}-\frac{T}{\beta_1^2\rho_0^2}\right)-\frac{1}{\beta_1^2}\left(-\frac{jk}{L}-\frac{1}{\rho_0^2}+T\right)T+\frac{1}{\rho_0^2}-T\right\}$$
$$\times\left\{\frac{1}{\beta_2^2}\left(\frac{1}{\rho_0^2}-\frac{T}{\beta_1^2\rho_0^2}\right)\left(\frac{1}{\beta_1^2\rho_0^4}-R\right)-\frac{T}{\beta_1^2\rho_0^2}+\frac{1}{\rho_0^2}\right\}+\frac{1}{\beta_2^2}\left[\left(-\frac{jk}{L}-\frac{1}{\rho_0^2}+T\right)\frac{1}{\beta_1^2\rho_0^2}+\frac{jk}{L}-\frac{1}{\rho_0^2}+R\right]$$
$$\times\left(\frac{1}{\beta_1^2\rho_0^4}-R\right)+\left(-\frac{jk}{L}-\frac{1}{\rho_0^2}+T\right)\frac{1}{\beta_1^2\rho_0^2}+\frac{1}{\rho_0^2}-R,$$

$$AA_x = \cos\ \varphi_n k\alpha_n r_0 \frac{2}{\beta_2^2\beta_1^2\rho_0^2}\left(\frac{1}{\rho_0^2}-\frac{T}{\beta_1^2\rho_0^2}\right)+\frac{k\alpha_m 2r_0\cos\varphi_m}{\beta_2^2}\left(\frac{1}{\rho_0^2}-\frac{T}{\beta_1^2\rho_0^2}\right)-\frac{\cos\varphi_n k\alpha_n r_0 2T}{\beta_1^2}+\cos\varphi_l k\alpha_l 2r_0,$$

$$CC_x = \frac{\mathrm{AA}_x}{\beta_3^2}\left\{\frac{1}{\beta_2^2}\left(\frac{1}{\rho_0^2}-\frac{T}{\beta_1^2\rho_0^2}\right)\left(\frac{1}{\beta_1^2\rho_0^4}-R\right)-\frac{T}{\beta_1^2\rho_0^2}+\frac{1}{\rho_0^2}\right\}+BB_x,$$

$$BB_x = \cos\varphi_n k\alpha_n r_0\frac{2}{\beta_2^2\beta_1^2\rho_0^2}\left(\frac{1}{\beta_1^2\rho_0^4}-R\right)+\frac{2}{\beta_2^2}k\alpha_m r_0\cos\varphi_m\left(\frac{1}{\beta_1^2\rho_0^4}-\mathrm{R}\right)+\cos\varphi_n k\alpha_n r_0\frac{2}{\beta_1^2\rho_0^2}+(\cos\varphi_o k\alpha_o 2r_0),$$

$$\begin{aligned}JJ_x = {}& \frac{AA_x}{2\beta_3^2}\left\{\frac{1}{\beta_2^2}\left[\left(-\frac{jk}{L}-\frac{1}{\rho_0^2}+T\right)\frac{1}{\beta_1^2\rho_0^2}+\frac{jk}{L}-\frac{1}{\rho_0^2}+R\right]\left(\frac{1}{\rho_0^2}-\frac{T}{\beta_1^2\rho_0^2}\right)-\frac{1}{\beta_1^2}\left(-\frac{jk}{L}-\frac{1}{\rho_0^2}+T\right)T+\frac{1}{\rho_0^2}-T\right\}\\ &+\frac{CC_x}{2\beta_4^2}B+\cos\varphi_n k\alpha_n r_0\frac{1}{\beta_2^2\beta_1^2\rho_0^2}\left[\left(-\frac{jk}{L}-\frac{1}{\rho_0^2}+T\right)\frac{1}{\beta_1^2\rho_0^2}+\frac{jk}{L}-\frac{1}{\rho_0^2}+R\right]\\ &+\frac{k\alpha_m r_0\cos\varphi_m}{\beta_2^2}\left[\left(-\frac{jk}{L}-\frac{1}{\rho_0^2}+T\right)\frac{1}{\beta_1^2\rho_0^2}+\frac{jk}{L}-\frac{1}{\rho_0^2}+R\right]+\frac{\cos\varphi_n k\alpha_n r_0}{\beta_1^2}\left(-\frac{jk}{L}-\frac{1}{\rho_0^2}+T\right),\end{aligned}$$

$$\begin{aligned}q_{2px} = {}& \frac{\cos\varphi_n k\alpha_n r_0}{\beta_1^2}\left(\frac{1}{\rho_0^2}-T\right)+\cos\varphi_n k\alpha_n r_0\frac{1}{\beta_2^2\beta_1^2\rho_0^2}\left[\frac{1}{\beta_1^2\rho_0^2}\left(\frac{1}{\rho_0^2}-T\right)+\frac{1}{\rho_0^2}-R\right]\\ &+\frac{k\alpha_m r_0\cos\varphi_m}{\beta_2^2}\left[\frac{1}{\beta_1^2\rho_0^2}\left(\frac{1}{\rho_0^2}-T\right)+\frac{1}{\rho_0^2}-R\right]+\frac{1}{2\beta_4^2}(CC_x D)+\frac{JJ_x KK}{2\beta_{1p}^2}\\ &+\frac{AA_x}{2\beta_3^2}\left\{\frac{1}{\beta_2^2}\left[\frac{1}{\beta_1^2\rho_0^2}\left(\frac{1}{\rho_0^2}-T\right)+\frac{1}{\rho_0^2}-R\right]\left(\frac{1}{\rho_0^2}-\frac{T}{\beta_1^2\rho_0^2}\right)-\frac{jk}{L}-\frac{1}{\rho_0^2}+T-\frac{T}{\beta_1^2}\left(\frac{1}{\rho_0^2}-T\right)\right\},\end{aligned}$$

$$\begin{aligned}KK = {}& \frac{1}{2\beta_3^2}\left\{\frac{1}{\beta_2^2}\left[\left(-\frac{jk}{L}-\frac{1}{\rho_0^2}+T\right)\frac{1}{\beta_1^2\rho_0^2}+\frac{jk}{L}-\frac{1}{\rho_0^2}+R\right]\left(\frac{1}{\rho_0^2}-\frac{T}{\beta_1^2\rho_0^2}\right)-\frac{1}{\beta_1^2}\left(-\frac{jk}{L}-\frac{1}{\rho_0^2}+T\right)T+\frac{1}{\rho_0^2}-T\right\}\\ &\times\left\{\frac{1}{\beta_2^2}\left[\frac{1}{\beta_1^2\rho_0^2}\left(\frac{1}{\rho_0^2}-T\right)+\frac{1}{\rho_0^2}-R\right]\left(\frac{1}{\rho_0^2}-\frac{T}{\beta_1^2\rho_0^2}\right)-\frac{jk}{L}-\frac{1}{\rho_0^2}+T-\frac{T}{\beta_1^2}\left(\frac{1}{\rho_0^2}-T\right)\right\}\\ &+\frac{1}{2\beta_2^2}\left[\left(-\frac{jk}{L}-\frac{1}{\rho_0^2}+T\right)\frac{1}{\beta_1^2\rho_0^2}+\frac{jk}{L}-\frac{1}{\rho_0^2}+R\right]\left[\frac{1}{\beta_1^2\rho_0^2}\left(\frac{1}{\rho_0^2}-T\right)+\frac{1}{\rho_0^2}-R\right]\\ &+\frac{1}{2\beta_4^2}BD+\frac{1}{2\beta_1^2}\left(-\frac{jk}{L}-\frac{1}{\rho_0^2}+T\right)\left(\frac{1}{\rho_0^2}-T\right)-2\left(T+R\right)+\frac{4}{\rho_0^2}.\end{aligned}$$

Here, AA_y, BB_y, CC_y, JJ_y, and q_{2py} are attained by, respectively, replacing all of the cos functions in AA_x, BB_x, CC_x, JJ_y, and q_{2px} by the sin functions.

Acknowledgments

Muhsin C. Gökçe, Yahya Baykal, Canan Kamacıoğlu, and Murat Uysal gratefully acknowledge the support provided by Çankaya University and Özyeğin University, respectively. Also all the authors are thankful to ICT COST Action IC1101 entitled "Optical Wireless Communications—An Emerging Technology." Muhsin C Gökçe also gratefully acknowledges the financial support from Tübitak 2211-C.

References

1. V. I. Tatarskii, *The Effects of the Turbulent Atmosphere on Wave Propagation*, National Technical Information Service, Springfield, Massachusetts (1971).
2. S. J. Wang, Y. Baykal, and M. A. Plonus, "Receiver–aperture averaging effects for the intensity fluctuation of a beam wave in the turbulent atmosphere," *J. Opt. Soc. Am.* **73** (6), 831–837 (1983).
3. X. Chu, Y. Ni, and G. Zhou, "Propagation analysis of flattened circular Gaussian beams with a circular aperture in turbulent atmosphere," *Opt. Commun.* **274** (2), 274–280 (2007).
4. S. Xueju et al., "Propagation analysis of flattened circular Gaussian beams with a misaligned circular aperture in turbulent atmosphere," *Opt. Commun.* **282** (24), 4765–4770 (2009).
5. R. Barrios and F. Dios, "Exponentiated Weibull distribution family under aperture averaging for Gaussian beam waves," *Opt. Express* **20**(12), 13055–13064 (2012).
6. C. Kamacıoğlu, Y. Baykal, and E. Yazgan, "Averaging of receiver aperture for flat-topped incidence," *Opt. Laser Technol.* **52**, 91–95 (2013).
7. C. Kamacıoğlu, Y. Baykal, and E. Yazgan, "Receiver–aperture averaging of annular beams propagating through turbulent atmosphere," *Opt. Eng.* **52**(12), 126103 (2013).
8. E. J. Lee and V. W. S. Chan, "Part 1: optical communication over the clear turbulent atmospheric channel using diversity," *IEEE J. Sel. Areas Commun.* **22** (9), 1896–1906 (2004).
9. M. Safari and Steve Hranilovic, "Diversity gain for near-field MISO atmospheric optical communications," in *Proc. IEEE Conf. on Communication*, 3128–3132 (2012).
10. S. M. Haas and J. H. Shapiro, "Capacity of wireless optical communications," *IEEE J. Sel. Area Commun.* **21**(8), 1346–1357 (2003).
11. E. J. Shin and V. W. S. Chan, "Optical communication over turbulent atmospheric channel using spatial diversity," in *Proc. IEEE Conf. on Global Telecommunications*, Vol. 1–3, pp. 2055–2060 (2002).
12. M. Safari and M. Uysal, "Diversity gain analysis of free-space optical communications systems," in *Proc. IEEE Conf. on Electrical and Computer Engineering*, Vol. 1–4, pp. 1239–1244 (2008).
13. S. M. Navidpour, M. Uysal, and M. Kavehrad, "BER performance of MIMO free-space optical transmission with spatial diversity," *IEEE Trans. Wireless Commun.* **6** (8), 2813–2819 (2007).

14. Ç. Arpali et al., "Intensity fluctuations of partially coherent laser beam arrays in weak atmospheric turbulence," *Appl. Phys. B* **103**(1), 237–244 (2011).
15. H. T. Eyyuboğlu, Y. Baykal, and Y. Cai, "Scintillation of laser array beams," *Appl. Phys. B* **91**(2), 265–271 (2008).
16. Y. Yuan et al., "Propagation factors of laser array beams in turbulent atmosphere," *J. Mod. Opt.* **57**(8), 621–631 (2010).
17. Y. Baykal, "Field correlations of laser arrays in atmospheric turbulence," *Appl. Opt.* **53**(7), 1284–1289 (2014).
18. Y. Baykal, H. T. Eyyuboğlu, and Y. Cai, "Scintillation of partially coherent multiple Gaussian beams in turbulence," *Appl. Opt.* **48** (10), 1943–1954 (2009).
19. I. S. Gradshteyn and I. M. Ryzhik, *Tables of Integrals, Series and Products*, Academic Press Inc. (2000).
20. L. C. Andrews, R. L. Philips, and C. Y. Hopen, *Laser Beam Scintillation with Application*, SPIE Press, Bellingham, WA (2001).
21. M. C. Gökçe et al., "Performance analysis of MIMO FSO systems with radial array beams and finite sized detectors," *Proc. SPIE* **9224**, 922409 (2014).

Muhsin C. Gökçe received his BSc in Electronic and Communication Engineering from Çankaya University, Ankara, Turkey, in 2009 and MS in Electrical and Electronics Engineering from Ankara University, Ankara, Turkey, in 2012. He is currently working towards a PhD in Electronic and Communication Engineering, Çankaya University. His current research interest is multiple-input multiple-output free space optical communications. He is working as a specialist in Çankaya University.

Yahya Baykal received his PhD from Northwestern University, Evanston, Illinois, in 1982. He worked as manager in R&D of Teletaş (Alcatel), Türk Philips Trades A.Ş. and as the general manager in İltek Telekomünikasyon (Iskratel) Company. He is currently vice rector in Çankaya University, Ankara, Turkey. He lectures in the areas of telecommunication networks. His main research areas cover atmospheric and underwater optical wireless systems. He is the author of 117 SCI and 58 conference papers.

Canan Kamacıoğlu received his BSc and MSc degrees from the Department of Electronic and Communication Engineering at Çankaya University Ankara, Turkey, and a PhD in electrical and electronics engineering from Hacettepe University in 2013. Her current research interests include free space optical communications, adaptive optics, and implementation of wireless optical systems. She is currently a part-time instructor at Çankaya University since 2013.

Murat Uysal is a full professor at Özyeğin University, İstanbul, Turkey, where he leads the Communication Theory and Technologies (CT&T) Research Group. Prior to joining Özyeğin University, he was a tenured associate professor at the University of Waterloo, Canada, where he still holds an adjunct faculty position. His research interests are in the broad areas of communication theory and signal processing, with a particular emphasis on the physical layer aspects of wireless communication systems in radio, acoustic, and optical frequency bands.